J Exp Biol Advance Online Articles. First posted online on 21 February 2013 as doi:10.1242/jeb.084194
Access the most recent version at http://jeb.biologists.org/lookup/doi/10.1242/jeb.084194

A cute and highly contrast-sensitive superposition eye - the diurnal owlfly *Libelloides macaronius*

[1]Gregor Belušič, [1,2]Primož Pirih, [3]Doekele G. Stavenga

[1]Department of Biology, Biotechnical faculty, University of Ljubljana, Ljubljana, Slovenia

[2]Department of Materials and Metallurgy, Faculty of Natural Sciences and Engineering, University of Ljubljana, Ljubljana, Slovenia

[3]Computational Physics, Zernike Institute for Advanced Materials, University of Groningen, Groningen, The Netherlands

Abstract

The owlfly *Libelloides macaronius* (Insecta: Neuroptera) has large bipartite eyes of the superposition type. The spatial resolution and sensitivity of the photoreceptor array in the dorsofrontal eye part was studied with optical and electrophysiological methods. Using structured illumination microscopy, the interommatidial angle in the central part of the dorsofrontal eye was determined to be $\Delta\varphi$ = 1.1°. Eye shine measurements with an epi-illumination microscope yielded an effective superposition pupil size of about 300 facets. Intracellular recordings confirmed that all photoreceptors were UV-receptors (λ_{max} = 350 nm). The average photoreceptor acceptance angle was 1.8°, with a minimum of 1.4°. The receptor dynamic range was two log units, and the Hill coefficient of the intensity-response function was n = 1.2. The signal-to-noise ratio of the receptor potential was remarkably high and constant across the whole dynamic range (RMS noise = 0.5% V_{max}). Quantum bumps could not be observed at any light intensity, indicating low voltage gain. Presumably, the combination of large aperture superposition optics feeding an achromatic array of relatively insensitive receptors with a steep intensity-response function creates a low-noise, high-spatial-acuity instrument. The sensitivity shift to the UV range reduces the clutter created by clouds within the sky image. These properties of the visual system are optimal for detecting small insect prey as contrasting spots against both clear and cloudy skies.

Keywords owlfly · interommatidial angle · superposition pupil · photoreceptor · acceptance angle · UV sensitivity · sky contrast

Introduction

The owlfly *Libelloides macaronius* (Scopoli, 1763) (formerly: *Ascalaphus macaronius*) (Insecta: Neuroptera: Ascalaphidae) is a predatory insect hunting above Ponto-Mediterranean meadows for small insect prey (Aspöck et al., 2001). The owlflies detect their prey as contrasting dark spots against the skies with the large dorsofrontal (DF) part of their compound eyes (Fig. 1A, B). Hunting activity is performed under bright light conditions, but quite surprisingly the dorsofrontal eyes are of the optical superposition type (Ast, 1920), considered to be characteristic for nocturnal and crepuscular invertebrates, like moths and crayfish (Land and Nilsson, 2002). Another remarkable property of the dorsofrontal eyes is that they are exclusively sensitive in the UV, which is due to the presence of only a single rhodopsin, with peak absorbance at 345 nm (measured spectrophotometrically in extracts), in all photoreceptor cells (Hamdorf, 1979).

The great hunting capacities of the owlflies indicate excellent spatial acuity as well as high signal-to-noise ratio and sensitivity of the compound eyes' photoreceptors. The spatial acuity depends on the interommatidial angle ($\Delta\varphi$), which determines the density of the eye's sampling points, and on the photoreceptor acceptance angle ($\Delta\rho$). High signal-to-noise ratio of photoreceptors is best achieved with a high light gathering capacity of the optical system (equivalent to a "bright lens" of a camera) and a low voltage gain of the photoreceptors (equivalent to a "low ISO" value of a camera sensor). Light absorption by the photoreceptors depends on the spatial acceptance angle of the photoreceptors and the absorbance of the photoreceptor's visual pigment, but predominantly on the size of the entrance pupil. Aberrations and diffraction widen the acceptance angle without increasing the photoreceptor sensitivity to extended light sources. Whereas in apposition eyes the entrance pupil is the cross-section of a single facet lens (Fig. 1G), in an optical superposition eye, where incident light from a point source reaches the photoreceptors via many facet lenses, the entrance pupil is much larger (Fig. 1D). The photon catch of the photoreceptors can thus be much improved, by up to three orders of magnitude (Warrant and McIntyre, 1993). However, a generally encountered drawback of superposition optics is that the eye's spatial acuity is inferior to that of apposition eyes (Warrant and McIntyre, 1990; Land and Nilsson, 2002).

The owlfly's predatory behaviour is similar to that of dragonflies (Fig. 1E; hence the derivation of the genus name *Libelloides*, "resembling *Libellula*"). Dragonflies are also aerial predatory insects catching insect prey while flying under bright light conditions, but they have apposition eyes (Fig. 1F) with dorsally predominantly blue-sensitive photoreceptors (Labhart and Nilsson, 1995). The recruitment of short-wavelength sensitive photoreceptors in the

upward-looking eye parts can be regarded as an optimisation in terms of matching the spectral sensitivity of the sensors to the spectral composition of the visual environment. Presumably this visual strategy also effectively reduces the intensity variations across the sky background. We hypothesize that the owlflies have driven this optimization to the extreme by employing photoreceptors that are exclusively sensitive in the UV and furthermore gained light sensitivity by using optical superposition imaging. Here we investigate these hypotheses with optical and electrophysiological experiments.

Materials and methods

Animals

Adult owlflies, *Libelloides macaronius*, were caught in the Slovenian part of the Karst. They were kept at a room temperature of 24 °C and regularly fed with liver or blowflies. For the laboratory experiments, which were all performed at room temperature, the animals were tethered to a copper yoke or plastic tubing and immobilized with a mixture of bees wax, resin and thermal conductive paste.

Structured illumination microscopy and interommatidial angle

The anatomical interommatidial angle was measured with a structured illumination microscope (SIM; ApoTome, Zeiss, Oberkochen, Germany) using a Zeiss 20× (NA 0.40) objective. This instrument projects a grating to the focal plane of the objective and computationally isolates the in-focus fluorescence in a thin planar section of a spatial object (Weigel et al., 2009). By making a stack of SIM images, the 3-dimensional distribution of an excited, fluorescent substance can be determined. Chitin, which constitutes the dioptric apparatus of the compound eye of *L. macaronius*, is distinctly green fluorescent under blue excitation light. We have used this fluorescence to determine the shape of the owlfly's dorsofrontal eyes. Locally the eyes approximated a sphere, and hence the radius of curvature, R, together with the local facet lens diameter, D, yields the interommatidial angle $\Delta\varphi = D/R$.

Eye shine and entrance pupil

The entrance pupil was determined with a telemicroscopic setup (Stavenga, 2002b), by measuring the owlfly's eye shine. The eye shine, which results from the reflection of incident light by the tapetal tracheoles that surround the rhabdoms, was photographed with a CoolSnap ES digital camera (Photometrics, Tucson, Az, USA). The illumination beam, aperture about 3°, entered the eye via only a few facets (spot diameter ca. 100 µm); the objective was a Zeiss

5× (NA 0.15). To suppress reflections on the objective lens surfaces, we used crossed polarizers.

Electrophysiological recordings, acceptance angle and spectral sensitivity

Intracellular recordings of photoreceptors in superposition eyes have proven to be notoriously difficult (Warrant et al., 1999; Warrant et al., 2003). For intracellular measurements of the photoreceptors in the owlfly eye, the mouth parts and muscles had to be removed in order to eliminate movements. A triangular hole was made in the cornea of an owlfly's right eye and sealed with Vaseline. Great care was taken to prevent the Vaseline from spreading around the cornea and corrupting the dioptrical apparatus. Borosilicate glass microelectrodes, pulled on a P-97 puller (Sutter Instrument Company, Novato, USA), were filled with 3 M KCl and had resistances 100-150 MΩ. The tip of the electrode, mounted at a PM-10 micromanipulator (Märzhäuser, Wetzlar, Germany), was inserted via the corneal hole into the eye. We succeeded in making reliable recordings in the dorsofrontal eye of the owlfly by advancing the electrode through the ~440 μm thick clear zone at an angle of maximally 30° with respect to the visual axis of the penetrated photoreceptors. This way the electrode was prevented from bending and clogging. The reference electrode was an Ag/AgCl wire positioned in the non-illuminated eye, screened from the stimulus. Successful photoreceptor impalement was characterized by a sudden drop in the electrode potential to the resting membrane potential and by a vigorous, directionally sensitive depolarisation upon UV illumination. In a typical run, a few photoreceptors of a single ommatidium could be penetrated, until the electrode broke when it touched the tracheolar sheath.

After penetration of a photoreceptor, its light sensitivity was measured by stimulation with a series of 380 nm-light pulses with graded light intensity. The angular sensitivity was measured by giving constant intensity light flashes, with interval 10 s, while changing the angular position of the light source after each flash in small angular steps (0.1 - 0.5°) passing through the optical axis. With the light source positioned at the cell's visual axis, the spectral sensitivity was measured by stimulation with a series of light pulses between 300 and 500 nm in 5 nm (or 1 nm) steps. The intensity of the light pulses was measured with a linear thermopile sensor (Newport Oriel, Irvine, USA) and the responses were corrected offline for the wavelength-dependent variations of the photon flux.

The light stimulator was for the angular sensitivity measurements a 380 nm, 350 mA LED (Roithner LaserTechnik, Wien, Austria) and for the spectral measurements a 150 W XBO lamp together with a shutter, a quartz condenser and lenses, a monochromator (77250-

M, Newport Oriel, Irvine, USA; bandpass FWHM ≈ 10 nm), a series of quartz neutral density filters (CVI Melles Griot, Didam, Netherlands), and a liquid light guide with quartz windows (Newport, Irvine, USA; diameter 5 mm). The end of the light guide was mounted at a perimetric device, and its aperture was defined by a narrow slit between the collimating quartz lens and the animal so that the light source subtended an angle < 0.1° at the preparation. The signal was amplified with a SEC-05 amplifier (npi electronic, Tamm, Germany), conditioned with a CyberAmp 320 (Molecular Devices, Sunnyvale, USA), digitized with a Micro 1401 lab interface (CED, Cambridge, UK) and recorded with the WinWCP software (John Dempster, University of Strathclyde, UK); see also Belušič et al. (2010).

Results

Interommatidial angle

We determined the interommatidial angle in the central part of the dorsofrontal eye of a living female owlfly by structured illumination microscopy (SIM; Fig. 2). By measuring optical sections at successive depths, a stack of sections was obtained from which the shape of the corneal surface was derived. Figure 2A-D shows consecutive micrographs, taken at the corneal level and 10, 20 and 40 μm below. The average facet lattice distance, measured along the facet rows, was $D = 31.5 \pm 0.5$ μm (see also Schneider et al., 1978). Figure 2E shows an eye scheme with the SIM section perpendicular to the corneal surface (XZ profile). The eye curvature in this part of the eye is slightly asymmetric, as indicated by the fact that the annuli of facets (Fig. 2A-D) are slightly ellipsoidal. The average curvature in the area of Fig. 2E where 32 facets spanned an arc of 36° was concluded to be $R = 1.60 \pm 0.08$ mm, thus yielding the interommatidial angle: $\Delta\varphi = D/R = 1.13 \pm 0.08°$.

Entrance pupil of the dorsofrontal eye

Each photoreceptor of an optical superposition eye receives light via a large number of facets (Fig. 1D). The assembly of facets relaying light to one and the same photoreceptor thus forms the entrance pupil. In principle, when compared to the apposition eye type (Fig. 1G), the number of facets making up the entrance pupil equals the optical gain factor of the superposition eye.

However, the different facets of the entrance pupil do not equally contribute. In an optical superposition eye, the dioptrical apparatus, consisting of corneal facet lenses and crystalline cones, is separated by the clear zone from the rhabdom layer (Figs. 1C, 2E, 3A). The rhabdoms are surrounded by air-filled tracheoles, which together constitute the tapetum. In

Figure 3A, a narrow-aperture light beam, entering a few facet lenses askew, is focused by the dioptric apparatus onto the central rhabdom, that is, the rhabdom of the ommatidium with visual axis parallel to the direction of illumination. A part of the light reaching the rhabdom layer is reflected by the tapetum and leaves the eye again. If the backscattering by the tapetum is diffuse, the effective entrance pupil can be deduced from the distribution of the reflected light flux, i.e. the eye shine. The reflected light flux is maximal via the central facet lens and progressively decreases towards the periphery (Fig. 3B), yielding the profile of Fig. 3C. We estimate that the effective entrance pupil is about 300 facets.

Photoreceptor acceptance angle and spectral sensitivity

The photoreceptor acceptance angle is a crucial quantity in determining the quality of an eye. We succeeded in measuring the acceptance angle of owlfly photoreceptors by intracellular recording. For cells to be accepted we put as criteria that the resting membrane potential was below -50 mV and that the maximal depolarization upon bright light flashes was about 30 mV or larger. In photoreceptors that were successfully impaled during a sufficiently long period (15 to 60 min), the intensity-response function, the angular sensitivity, and the spectral sensitivity were measured.

All photoreceptors recorded were exclusively sensitive in the ultraviolet wavelength range. The light intensity – photoreceptor response relation (the V – log I curve) was measured with 300 ms UV flashes, wavelength λ = 380 nm, over an intensity range of 6 log units. The recorded receptor potentials were remarkably smooth (Fig. 4A) without discernible quantum bumps even in dim light. Increasingly intense flashes created an increasing depolarization with a moderate peak to plateau transition. At the most intense flashes, the depolarization was followed by a minor hyperpolarization. The receptor potential amplitude, plotted as a function of the light flash intensity and fitted with a Hill function (Fig. 4B),

$$V(I) = I^n/(I^n_{50} + I^n) \quad (1)$$

yielded a Hill slope of n = 1.18 ± 0.10 (12 recorded cells).

The angular sensitivity was measured by stimulation with constant intensity light flashes, interval 10 s, while changing the angular position of the < 0.1° light source after each flash in small angular steps (0.1 - 0.5°). The amplitude of the obtained receptor potential then was converted into sensitivity using the inverse Hill function. The obtained angular sensitivity function was always bell-shaped; it was symmetrical and identical when measured along the vertical as well as the horizontal axis (Fig. 4C). The central part of the angular sensitivity function could be well fitted with a Gaussian function, with average halfwidth

$\Delta\rho$ = 1.77 ± 0.09° (N = 8), but the curves deviated from a Gaussian in the tail. Figure 4C shows the angular sensitivity of the cell with the narrowest acceptance angle, $\Delta\rho$ = 1.40°. The cells with larger $\Delta\rho$ - values were presumably located marginally in the retina, where the eye radius, *R*, steeply drops and the interommatidial angle, $\Delta\varphi$, increases. In other words, the $\Delta\rho$ values which were much larger than the mean probably resulted from the complex curvature of the eye. Consequently, the average acceptance angle, $\Delta\rho$, of all measured cells was substantially larger than the minimal $\Delta\rho$.

The spectral sensitivity was measured in a 5-nm or 1-nm step spectral scan, delivering light flashes with duration 300 ms and with interval 5 s. The wavelength-dependent amplitudes of the elicited receptor potentials were converted, using the inverse Hill function, into the spectral sensitivity. The resulting spectrum was then fitted with a rhodopsin template (Stavenga, 2010), yielding a peak wavelength 349.8 ± 0.2 nm (N = 4; Fig. 4D).

Discussion

The neuropteran family Ascalaphidae consists of two subfamilies, the Ascalaphinae and the Haplogleniinae. The members of the Haplogleniinae subfamily have undivided eyes (no sulcus) and are active during the dark. The species of the Ascalaphinae subfamily have divided (sulcate) eyes and share both crepuscular and diurnal lifestyles (Fischer and Kral., 2006). The whole family has optical superposition eyes (Ast, 1920), an eye type mostly found in nocturnal and crepuscular insects (Nilsson, 1989). Nevertheless, several cases of diurnal insects with superposition eyes are well known, such as the agaristid moths, skipper butterflies (Horridge et al., 1972), sphingid moths (Exner, 1891; Warrant et al., 1999), certain neuropterans such as *Mantispa styriaca* (Eggenreich and Kral, 1990; Kral et al., 2000), *Palpares libelluloides* (own observation), and some beetles (McIntyre and Caveney, 1985). As these diurnal groups are often more or less closely related to extant nocturnal groups, it is commonly assumed that these cases represent former nocturnal animals, which retained the ancestral optical design despite the transition to a diurnal lifestyle. The origin of the apposition and superposition eye and their transition is not clear, however (Nilsson 1989, Land and Nilsson 2002).

The superposition optics increases the eye sensitivity, but potentially at a price of decreased spatial resolution due to accumulation of optical errors of the many facets contributing to the superposition pupil. As a consequence, the photoreceptor acceptance angle is often substantially wider than the interommatidial angle ($\Delta\rho >> \Delta\varphi$), resulting in oversampling (Snyder, 1977; Snyder 1979; Land, 1997). We note that we attempted

intracellular recordings in the ventrolateral eye as well, but the success rate was low, and the results were puzzling since the acceptance angle was always much wider than the interommatidial angle ($9° < \Delta\rho < 22°$; $\Delta\varphi \approx 3°$); at this stage, we cannot rule out that this was due to distortions resulting from the electrophysiological methods.

High visual acuity (or oversampling: $\Delta\rho > 2\Delta\varphi$; Land, 1997) has been documented in superposition eyes for nocturnal moths (*Deilephila elpenor:* $\Delta\rho = 3°$; $\Delta\varphi = 1.3°$; Warrant et al., 2003; Theobald et al., 2010), crepuscular butterflies (*Caligo memnon*: $\Delta\rho_{DA} = 2.06°$; $\Delta\varphi = 0.8°$; Frederiksen and Warrant, 2008) and in certain skipper butterflies (*Toxidia peroni:* $\Delta\rho = 6\sim8°$, $\Delta\varphi = 1.9°$; Horridge et al., 1972). Oversampling apposition eyes have been encountered in the case of nocturnal bees, which have considerably enlarged fused rhabdoms. On the other hand, matched sampling (Land, 1997) or undersampling ($\Delta\rho \leq 2\Delta\varphi$) with high spatial resolution has been demonstrated in nocturnal (*Epargyrus clarus:* $\Delta\rho = 2.1°$, $\Delta\varphi = 1.3°$; Døving and Miller, 1968) and diurnal moths with superposition eyes (*Phalaenoides tristifica*: $\Delta\rho \approx 1.7°$; $\Delta\varphi \approx 2.0°$; Horridge et al., 1977; Warrant et al., 2003). An extreme case is the hummingbird hawkmoth *Macroglossum stellatarum*, which has aspherical compound eyes with a larger number of facets than rhabdoms, and photoreceptors with acceptance angle $\Delta\rho = 1.3°$, the narrowest ever measured to date in a superposition eye (Warrant et al., 1999; Warrant, personal communication).

Unquestionably, when a superposition eye has the same spatial acuity as its apposition counterpart, its optics is preferable because it collects more light through the increased superposition pupil. The optical aberrations of a superposition eye can be reduced by increasing the effective F-ratio with an enlarged clear zone. The dorsal eye part in the owlfly exhibits a remarkably elongated clear zone, if compared with the ventral part (Fig. 1C). A feature likely to improve the visual acuity of a superposition eye is the partial coherence of light entering through groups of facets in the superposition aperture (Stavenga, 2006). An important structure enhancing the acuity of a superposition eye is the tracheolar sheath surrounding each ommatidium at the level of the rhabdom, which prevents leakage of light to neighbouring ommatidia. The extensively developed tracheolar sheath in the owlfly eye shows that the optical isolation of ommatidia is tight, suggesting that this superposition eye is specialized for functioning in diurnal conditions (Schneider et al., 1978). The tracheolar sheath also creates a mirrored box around the rhabdom, thus increasing the capture of photons from the oblique rays at the aperture's periphery. Our present results demonstrate that the dorsofrontal eyes of the owlfly *L. macaronius* have indeed achieved a high spatial acuity ($\Delta\rho_{min} = 1.4°$, $\Delta\varphi_{min} = 1.1°$). Interestingly, the eyes of both *L. macaronius* and *M. stellatarum*

have a high spatial acuity even when compared with butterflies with apposition eyes of a comparable size (van Hateren and Nilsson, 1987; Frederiksen and Warant, 2008), in spite of the relatively large size of the superposition pupil (300 to 350 facets, respectively).

The physiologically measured receptor acceptance angle in the owlfly shows substantial flanks. These are probably caused by stray light (Fig. 4C), a likely side effect of the accumulated optical imperfections in the large array of dioptrical apparatuses contributing to the aperture of a photoreceptor. The broadened angular sensitivity is likely an acceptable compromise, given the high increase in aperture size, allowing a low transduction gain. Within the operating dynamic range of the photoreceptor response, the low photon shot noise results in an excellent signal-to-noise ratio, and therefore a very low contrast detection threshold. Tiny variations in light intensity can thus be reliably resolved. In other words, the steep intensity-response relation and the narrow dynamic working range means that the apparent contrast of the visual environment is increased by the large voltage gain.

Our field observations demonstrated that the owlflies react to objects covering a spatial angle much less than a degree. For example, a large flying ant, which is a typical prey of the owlfly, flying at a distance of 2 m can trigger rapid take-off. Such an insect, with a 5 mm diameter silhouette spanning an angle < 0.1°, will obscure only a small fraction of the visual field of a photoreceptor. It will cause a decrease in the captured light flux by ca. 1%. Assuming that the photoreceptor operates in the middle of its dynamic range, this light flux decrease will elicit a change in the receptor potential of < 0.15 mV (0.3% V_{max}). A moving object creating such a small contrast can only be reliably detected by an array of photoreceptors operating with minimal noise and high contrast gain, feeding a high-quality input to the neural circuitry performing movement detection.

We have quantified the signal to noise ratio (SNR) of the measured receptor potentials by calculating the root mean square (RMS) of the photoreceptor signal and normalizing the RMS to the maximal receptor depolarization, V_{max}. The photoreceptor response of *L. macaronius* was smooth at any applied light intensity and only slightly noisier than the time course in the dark. The average RMS-value varied between 0.42 ± 0.03% V_{max} and 0.52 ± 0.03% V_{max} at low and high intensities, respectively (N = 6). In order to compare these values with published data on dragonfly photoreceptors, we estimated the peak-to-peak voltage noise range ($V_{p\text{-}p}$ [% V_{max}]) by multiplying the RMS with 4. Assuming Gaussian distribution of noise, the estimated range thus contained the central 95.4% of samples. Figure 5 presents the owlfly data together with the data from the UV- and green-sensitive photoreceptors of the dragonfly *Hemicordulia tau* (Fig. 1E; Laughlin, 1976). The UV-

photoreceptors of *L. macaronius* and the green-sensitive photoreceptors of *H. tau* have a very similar voltage noise, while the UV-photoreceptors of *H. tau* are much noisier. The latter is attributed to the much higher phototransduction gain in the UV receptors, which presumably makes up for the lower UV light flux into an apposition eye in the normal diurnal environment (Laughlin, 1976). The owlfly clearly has resolved that problem by employing a superposition eye design.

We note here that the owlfly photoreceptors were recorded at 24 °C, a temperature at least 10 degrees lower than the working temperature in the field, ca 35-40 °C (Belušič et al., 2008). The owlfly's photoreceptor response latency to a light pulse is reduced from ~12 ms at 24 °C to ~4 ms at 38 °C, the ERG flicker fusion frequency at these two temperatures is 75 and 250 Hz, respectively (Belušič et al., 2008), and the receptor potential RMS noise is 1.6 times higher at 38 °C (Pirih and Belušič, unpublished). Even taking this into account, the noise of the owlfly's UV receptor is still much lower than the noise of the dragonfly's counterpart.

Dragonflies have dorsal eye parts with blue receptors, which are combined with reddish screening pigments, located distally in the eye (Stavenga, 1992; Labhart and Nilsson, 1995). This combination is related to the special photochemistry of invertebrate visual pigments, namely that the photoproduct of the native rhodopsin, metarhodopsin, is bathochromic shifted, thus allowing photoreconversion of the metarhodopsin back to its native state by long-wavelength light leaking through the distal pigment screen (Stavenga, 2002a). Prolonged irradiation of these visual pigments with white or wide-spectral-band light results in a photosteady state with a high rhodopsin content (Hamdorf, 1979). Photoconversion of the owlfly UV-rhodopsin with λ_{max} = 345 nm results in a metarhodopsin with peak wavelength λ_{max} = 480 nm (Hamdorf, 1979). The extreme bathochromic shift of the metarhodopsin together with the low UV-content of natural light compared to the blue-green wavelength range will result in a photosteady state with negligible depletion of rhodopsin, even without the presence of long-pass screening pigments. The dark brown screening pigment of the owlfly exhibits modest long-pass characteristics in the orange-red part, where metarhodopsin absorbance is negligible (Schneider et al., 1978).

Eye regionalization with a complete sensitivity shift towards short wavelength light in the dorsal eye part is common in insects that hunt prey or chase conspecifics against the skies (e.g., mayflies, Horridge and McLean, 1978; drone bees, Peitsch et al., 1992). An obvious hypothesis for spectral sensitivities peaking in the blue is that the photoreceptors are tuned for maximal background detection and rendering the prey to appear as contrastful dark spots. However, the photoreceptors in the dorsofrontal eye of the owlfly are maximally sensitive in

the UV and therefore the tuning must be other than merely for maximal light catch since skylight contains less UV than blue.

A likely reason is suggested by Figure 6, which shows that the intensity contrasts of a sparsely clouded sky decrease with decreasing wavelength. White clouds create less contrast in the blue than in green or red because of wavelength-independent Mie scattering on the water droplets of the clouds, which effectively redistributes both sky and direct sun beam radiation. Even the clear skies are more uniformly lit in the UV part of the spectrum (Dave, 1978; Pirih, unpublished data). Thus, tuning the eye to UV is likely to simplify the visual environment above, which may represent a distinct evolutionary driving force for the shift of vision towards the extreme short wavelengths of the light spectrum, favouring an achromatic, UV-sensitive eye. However, the apposition optics of the eyes of other aerial predators, like the dragonflies, may prohibit such a shift of sensitivity to the UV, since their photoreceptors would capture too little photons and thus suffer from a low signal-to-noise ratio. Blue receptors may therefore be optimal for dragonflies (Labhart and Nilsson, 1995). In the case of the owlfly, the superposition optics compensates for the low UV photon flux. Presumably, the ancestral, nocturnal owlflies had superposition eyes which *Libelloides macaronius* retained, thus allowing the employment of acute and highly contrast-sensitive, pure UV receptors, which serve well in effective prey capture under both sunny and clouded light conditions.

Acknowledgments

We are grateful to Drs Kazimir Drašlar for providing the SEM image and the owlfly eye section, Simon Laughlin for the dragonfly eye section, Aleš Kladnik for performing the structural illumination microscope (ApoTome) measurements, Navinda Kottege for the dragonfly photo and Hein Leertouwer for the sky photography. Two referees helped to improve the manuscript by giving ample constructive comments.

Funding

This study was supported in part by the Air Force Office of Scientific Research/European Office of Aerospace Research and Development AFOSR/EOARD (grant FA8655-08-1-3012 to DGS).

References

Aspöck, H., Holzel, H. and Aspöck, U. (2001). Kommentierter Katalog der Neuropterida (Raphidioptera, Megaloptera, Neuroptera) der Westpaläarktis. *Denisia* **2**, 1-606.

Ast, F. (1920). Über den feineren Bau der Facettenaugen bei Neuropteren. *Zool. Jb. Anat.* **41**, 411-458.

Belušič, G., Škorjanc, A. and Zupančič, G. (2008). Temperature dependence of photoreception in *Ascalaphus* (*Libelloides macaronius*; Insecta: Neuroptera). *Acta Biol. Slov.* **50**, 93-101.

Belušič, G., Pirih, P. and Stavenga, D. G. (2010). Photoreceptor responses of fruitflies with normal and reduced arrestin content studied by simultaneous measurements of visual pigment fluorescence and ERG. *J. Comp. Physiol. A* **196**, 23-35.

Dave, J.V. (1978) Extensive datasets of the diffuse radiation in realistic atmospheric models with aerosols and common absorbing gases. *Solar Energy* **21**: 361-369.

Døving, K.B. and Miller, W.H. (1968)**.** Function of insect compound eyes containing crystalline tracts. *J. Gen. Physiol.* **54,** 250-267.

Eggenreich, U. and Kral, K. (1990). External design and field of view of the compound eyes in a raptorial neuropteran insect, *Mantispa styriaca*. *J. Exp. Biol.* **148**, 353-365.

Exner, S. (1891). Die Physiologie der facittirten Augen von Krebsen und Insecten. Leipzig: Deuticke.

Fischer, K., Hölzel, H. and Kral, K. (2006). Divided and undivided compound eyes in Ascalaphidae (Insecta, Neuroptera) and their functional and phylogenetic significance. *J. Zool. Syst. Evol. Res.* **44**, 285-289.

Frederiksen, R. and Warrant, E.J. (2008). Visual sensitivity in the crepuscular owl butterfly *Caligo memnon* and the diurnal blue morpho *Morpho peleides*: a clue to explain the evolution of nocturnal apposition eyes? *J. Exp. Biol.* **211**, 844-51

Hamdorf, K. (1979). The physiology of invertebrate visual pigments. In: H. Autrum (ed.), *Handb. Sens. Physiol. Vol.* VII/6A, pp. 145-224. Berlin Heidelberg New York, Springer.

Hateren van, J.H. and Nilsson, D.-E. (1987) Butterfly optics exceed the theoretical limits of conventional apposition eyes. *Biol. Cybern.* **57**, 159-168

Horridge, G. A., Giddings, C. and Stange, G. (1972). The superposition eye of skipper butterflies. *Proc. R. Soc. Lond. B* **182**, 457-495.

Horridge, G.A., McLean, M., Stange, G., Lillywhite, P.G. (1977) A diurnal moth superposition eye with high resolution *Phalaenoides tristifica* (Agaristidae). *Proc. R. Soc. Lond. B* **196,** 233-50.

Horridge, G. A. and McLean, M. (1978). The dorsal eye of the mayfly *Atalophlebia* (Ephemeroptera). *Proc. R. Soc. Lond B* **200**, 137-150.

Kral, K., Vernik, M. and Devetak, D. (2000). Visually controlled prey-capture behaviour of the European mantispid, *Mantispa styriaca*. *J. Exp. Biol.* **203**, 2117-2123.

Labhart, T. and Nilsson, D.-E. (1995). The dorsal eye of the dragonfly *Sympetrum*: specializations for prey detection aginst the blue sky. *J. Comp. Physiol. A* **176**, 437-453.

Land, M. F. (1997). Visual acuity in insects. *Annu. Rev. Entomol.* **42**, 147-177.

Land, M. F. and Nilsson, D.-E. (2002). Animal eyes. Oxford: Oxford University Press

Laughlin, S.B. (1976). The sensitivities of dragonfly photoreceptors and the voltage gain of transduction. *J. Comp. Physiol. A* **111**, 221-247.

McIntyre, P. D. and Caveney, S. (1985). Graded-index optics are matched to optical geometry in the superposition eyes of scarab beetles. *Phil. Trans. R. Soc. Lond. B* **311**, 237-269.

Nilsson, D.-E. (1989). Optics and evolution of the compound eye. In: *Facets of vision* (eds. Stavenga, D. G. and Hardie, R. C.), pp. 30-73. Berlin Heidelberg: Springer.

Peitsch, D., Fietz, A., Hertel, H., de Souza, J., Ventura, D. F. and Menzel, R. (1992). The spectral input systems of hymenopteran insects and their receptor-based colour vision. *J. Comp. Physiol. A* **170**, 23-40.

Schneider, L., Gogala, M., Drašlar, K., Langer, H. and Schlecht, P. (1978). Feinstruktur und Schirmpigment-Eigenschaften der Ommatidien des Doppelauges von *Ascalaphus* (Insecta, Neuroptera). *Eur. J. Cell. Biol.* **16**, 274-307.

Snyder, A. W. (1977). Acuity of compound eyes: physical limitations and design. *J Comp Physiol* **116,** 161-182.

Snyder, A. W. (1979). The physics of compound eyes. In: H. Autrum (ed.) *Handb. Sens. Physiol., Vol* VII/6A, pp. 225-313., Berlin Heidelberg New York, Springer

Stavenga, D. G. (1992). Eye regionalization and spectral tuning of retinal pigments in insects. *Trends Neurosci.* **15**, 213-218.

Stavenga, D. G. (2002a). Colour in the eyes of insects. *J. Comp. Physiol. A* **188**, 337-348.

Stavenga, D. G. (2002b). Reflections on colourful butterfly eyes. *J. Exp. Biol.* **205**, 1077-1085.

Stavenga, D. G. (2006). Partial coherence and other optical delicacies of lepidopteran superposition eyes. *J. Exp. Biol.* **209**, 1904-1913.

Stavenga, D. G. (2010). On visual pigment templates and the spectral shape of invertebrate rhodopsins and metarhodopsins. *J. Comp. Physiol. A* **196**, 869-878.

Theobald, J. C., Warrant, E. J,. and O'Carroll, D. C. (2010). Wide-field motion tuning in nocturnal hawkmoths. *Proc R. Soc. B.* **277**, 853-60.

Warrant, E., Bartsch, K. and Gunther, C. (1999). Physiological optics in the hummingbird hawkmoth: A compound eye without ommatidia. *J. Exp. Biol.* **202**, 497-511.

Warrant, E. J., Kelber, A. and Kristensen, N. P. (2003). Eyes and vision. In: *Handbook of Zoology, Vol. IV, Part 36, Lepidoptera, Moths and Butterflies, Vol 2: Morphology, physiology and development* (ed. Kristensen, N. P.), pp. 325-359. Berlin New York: Walter de Gruyter.

Warrant, E. J. and McIntyre, P. D. (1990). Limitations to resolution in superposition eyes. *J. Comp. Physiol. A* **167**, 785-803.

Warrant, E. J. and McIntyre, P. D. (1993). Arthropod eye design and the physical limits to spatial resolving power. *Prog. Neurobiol.* **40**, 413-461.

Weigel, A., Schild, D. and Zeug, A. (2009). Resolution in the ApoTome and the confocal laser scanning microscope: comparison. *J. Biomed. Opt.* **14**, 014022.

Figure captions

Fig. 1. **A** Photograph of a female owlfly *Libelloides macaronius* in a typical basking position, warming up before starting a flight in the morning. **B** Scanning electron microscope photograph of the right compound eye (lateral view, dorsal side up), showing the clear sulcus, dividing the dorsofrontal (DF) from the ventrolateral (VL) part. **C** A histological section of the eye between the red and blue dots in **B**, showing its superposition structure, with from distal to proximal the dioptrical apparatus (da), with the corneal facet lenses and the crystalline cones, the clear zone (cz), and the rhabdom layer (rl). **D** Diagram of a superposition eye, with the light rays from infinity entering multiple facets through the corneal lenses (c), crystalline cones (cc) and clear zone (cz), being focussed into a single rhabdom in the rhabdom layer (rl). **E** The dragonfly Tau emerald, *Hemicordulia tau*, with its prominent compound eyes, regionalized into the red-pigmented dorsal retina and the yellow-green pigmented ventral retina. **F** Section of an eye of *H. tau*, in a plane indicated by the red and blue dots in **F**, showing the eye's apposition structure (Va and Vp, anterior posterior of the ventral retina; D, dorsal retina; the black lines indicate the border between the two retinal parts; da, dioptrical apparatus, rl, rhabdom layer). **G** Diagram of an apposition eye with light rays entering a rhabdom through a single corneal lens (c) and crystalline cone (cc; rl, rhabdom layer). Scale bar: **A**, 1 cm; **B**, **C**, 0.5 mm, **E**, 3 mm, **F**, 200 μm.

Fig. 2. Corneal facet lens pattern obtained with structural illumination microscopy (SIM) of a living specimen. **A-D** SIM sections at 0, 10, 20, and 40 μm from the corneal level; bar, 100 μm. **E** Longitudinal section of the facet lenses derived computationally from a series of perpendicular sections like those of A-D. The eye radius was derived by fitting the facet lenses with an arch as indicated. Bar, 100 μm.

Fig. 3. Eyeshine of the eye of *Libelloides macaronius*. **A** Diagram of the light distribution in the eye due to illumination with a small aperture light source of essentially one facet lens. Due to a gradient refractive index in the facet lens and cone, light is diverted onto the rhabdom of the central ommatidium, with visual axis parallel to the direction of the illumination. The rhabdoms are surrounded by a light reflecting and scattering tapetum, created by air-filled tracheoles, so that part of the incident light is backscattered and leaves the eye again as the eye shine. **B** Eye shine created by off-axis illumination of a few facets (bright spot). Scale bar, 100 μm. **C** Horizontal intensity profile of the eye shine. The profile of a

single row (thin line; dashed region of B) is modulated by individual facets. The profile of four rows (thick line; region delineated with a solid line in B) shows that the shape of the superposition pupil resembles a capped cone. The cap radius and the flank annulus are both about seven facets wide.

Fig. 4. Examples of receptor potentials and sensitivity of an owlfly photoreceptor. **A** Responses to 300 ms light flashes, wavelength λ = 380 nm, graded in 0.5 log intensity steps. **B** Amplitudes of the evoked receptor potentials as a function of the log (normalized light intensity), $\log(I/I_{max})$. The data were fitted with a Hill function (Eq. (1)). **C** Angular sensitivity measured with angular steps 0.1° fitted with a Gaussian function. Its half-width is the acceptance angle, $\Delta\rho$. **D** Spectral sensitivity measured in four cells with 1 nm steps fitted with a rhodopsin template.

Fig. 5. Noise levels (mean ± SD) in photoreceptors of insect aerial predators. The data of the UV receptors of the owlfly *Libelloides macaronius* (*Lm*; N = 6) is compared with those for the UV and green (G) receptors of the dragonfly *Hemicordulia tau* (*Ht*; from Laughlin, 1976).

Fig. 6. The wavelength dependence of the contrast between clouds and sky. **A** A normal RGB photograph. **B-G** The R, G, and B channels of **A**. **E** The R channel of a photograph taken with a UV filter (Schott glasses UG3 and BG17). **F** The normalized intensity distributions of **B**-**E**.

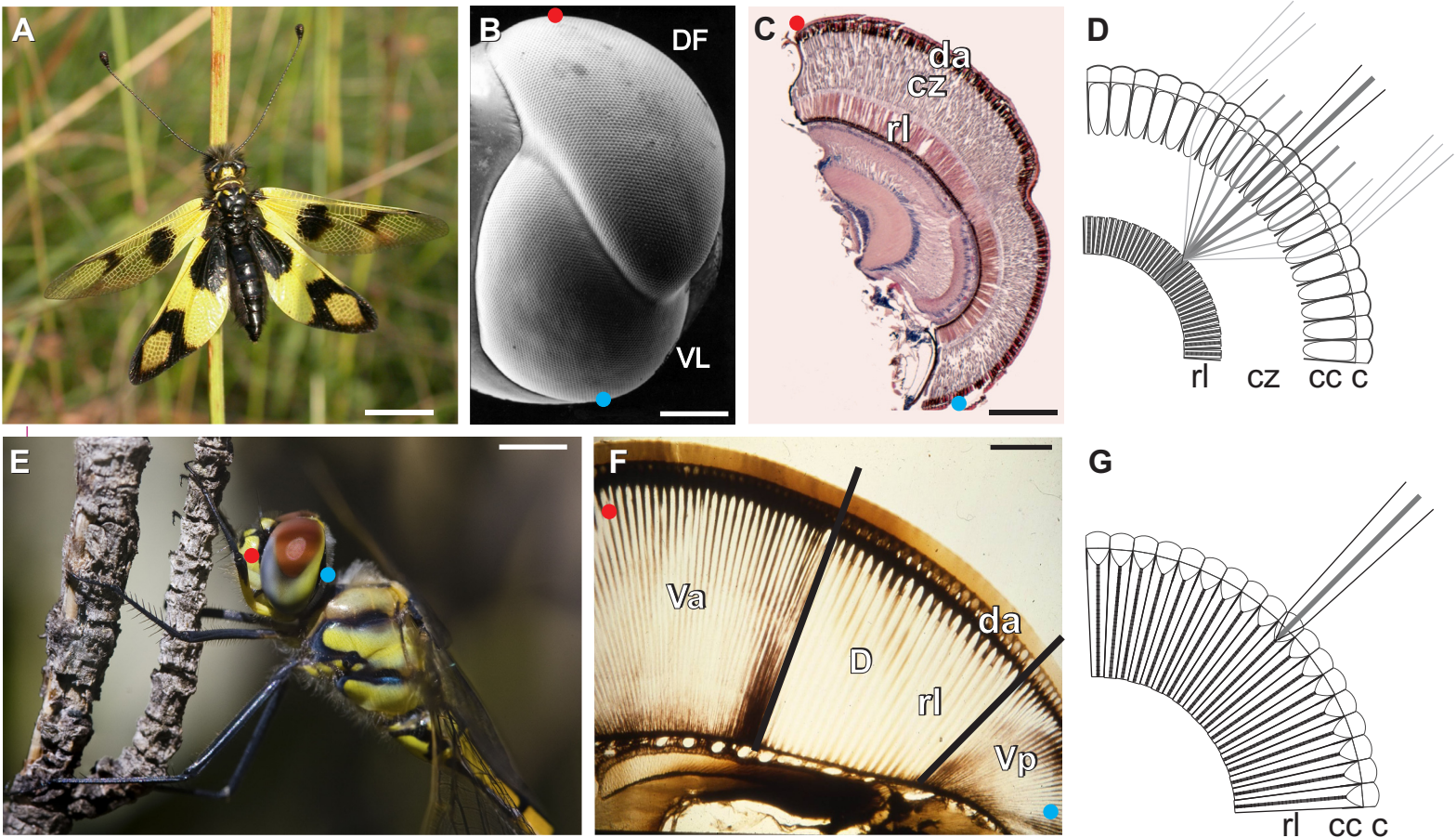
A
B
DF
VL
C
da
cz
rl
D
rl
cz
cc c
E
F
Va
D
da
rl
Vp
G
rl
cc c

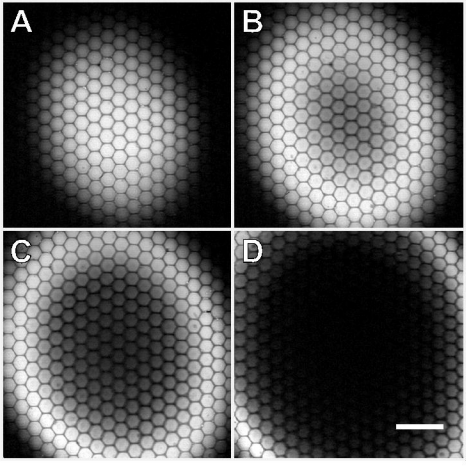
A
B
C
D
E
c
cc
cz
rh

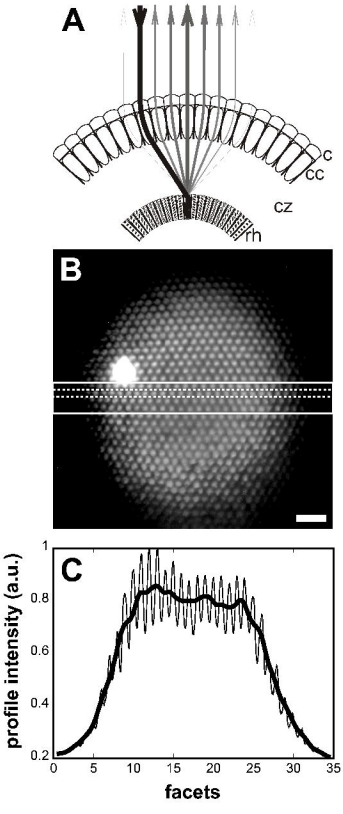
A
c
cc
cz
rn
B
C
profile intensity (a.u.)
1
0.8
0.6
0.4
0.2
0
5
10
15
20
25
30
35
facets

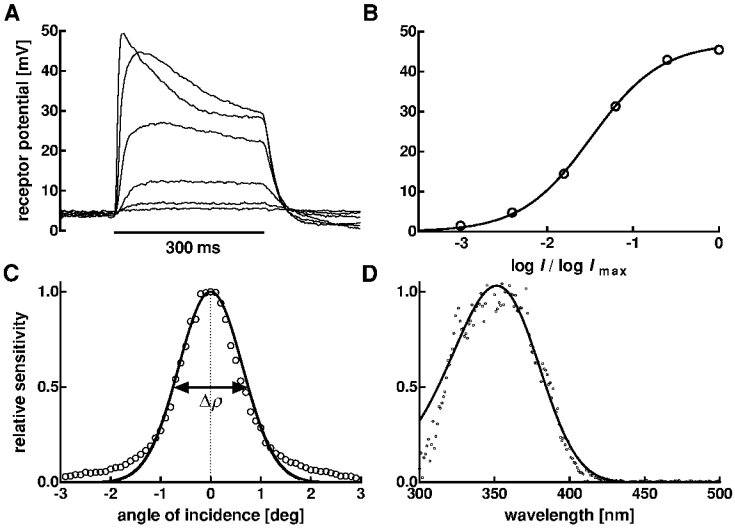
A
receptor potential [mV]
50
40
30
20
10
0
300 ms
B
50
40
30
20
10
0
-3
-2
-1
0
log I / log I max
C
relative sensitivity
1.0
0.5
0.0
Δρ
-3
-2
-1
0
1
2
3
angle of incidence [deg]
D
1.0
0.5
0.0
300
350
400
450
500
wavelength [nm]

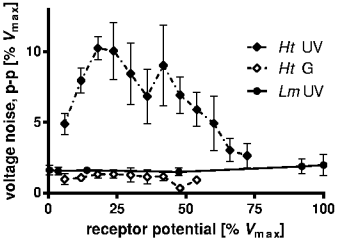
voltage noise, p-p [% V_{max}]
10
5
0
0
25
50
75
100
receptor potential [% V_{max}]
Ht UV
Ht G
Lm UV

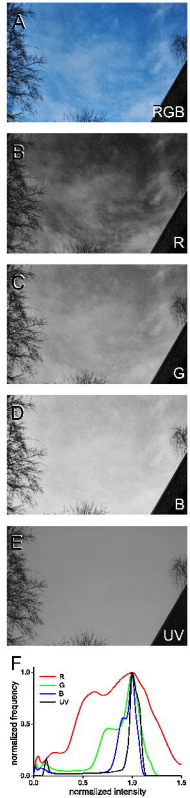
A
RGB
B
R
C
G
D
B
E
UV
F
R
G
B
UV
normalized frequency
normalized intensity
0.0
0.5
1.0
1.5

Table I: Parameters of the photoreceptor cells used in the analysis (Mean ± S.E.M.)

Symbol	parameter	unit	value
λ_{max}	spectral sensitivity maximum	nm	349.8 ± 0.2
V_m	resting membrane potential	mV	57.0 ± 3.3
V_{max}	maximal depolarization	mV	32.0 ± 2.7
n	Hill slope of the V-log$I$ curve		1.18 ± 0.10
RMS_D	average noise in the dark	% V_{max}	0.42 ± 0.03
RMS_L	maximal noise in the light	% V_{max}	0.52 ± 0.03
V_{p-p}	Peak-to-peak noise in the dark (95% range)	% V_{max}	1.34 ± 0.06
V_{p-p}	Peak-to-peak noise in the light (95% range)	% V_{max}	1.98 ± 0.75
$\Delta\rho$	acceptance angle	°	1.77 ± 0.09
$\Delta\varphi$	interommatidial angle	°	1.13 ± 0.08